Condensation and coagulation sinks and formation of nucleation mode particles in coastal and boreal forest boundary layers

M. Dal Maso, M. Kulmala, K. E. J. Lehtinen, J. M. Mäkelä,[1]
P. Aalto, and C. D. O'Dowd[2]
Department of Physical Sciences, University of Helsinki, Finland

Received 6 July 2001; revised 28 November 2001; accepted 17 December 2001; published 13 August 2002.

[1] The formation and growth of new particles has been evaluated using a revised version of a simple, but novel, theoretical tool. The concentration of condensable vapors and their source rates has been estimated using the aerosol condensation sink together with the measured particle growth rate. Also, by adding the coagulation sink and the measured formation rate of 3 nm particles, the formation rate of 1 nm particles and their concentration can be estimated. Condensation and coagulation sinks can be obtained from ambient aerosol size distribution data. The method has been applied to analyze the particle formation and growth rates observed during coastal and boreal forest nucleation events. The condensation sinks are typically $4-7 \times 10^{-3}$ s^{-1} in the forest and 2×10^{-3} s^{-1} under coastal conditions, while the coagulation sinks for 1, 2, and 3 nm particles are typically smaller by factors 1.5–2, 5–7, and 11–15, respectively. The measured growth rates are 2–10 nm/h for the boreal forest and range from 15 to 180 nm/h at the coast, corresponding to a vapor concentration of $2-13 \times 10^7$ cm^{-3} and 10^8 cm^{-3} to 10^9 cm^{-3}, respectively. The vapor source rate was $1-2 \times 10^5$ cm^{-3}s^{-1} in the boreal forest and $2-5 \times 10^6$ cm^{-3}s^{-1} in the coastal environment. The estimated formation rate of 1 nm particles in the forest environment was 8–20 cm^{-3}s^{-1} and 300–10,000 cm^{-3}s^{-1} at the coast. The concentration of 1 nm particles was estimated to be 2000–5000 and $4 \times 10^4-7 \times 10^6$ particles cm^{-3} in forest and at coast, respectively. *INDEX TERMS:* 0305 Atmospheric Composition and Structure: Aerosols and particles (0345, 4801); 0365 Atmospheric Composition and Structure: Troposphere—composition and chemistry; 0322 Atmospheric Composition and Structure: Constituent sources and sinks; *KEYWORDS:* coagulation, condensation, particle formation, nucleation

1. Introduction

[2] Atmospheric aerosol particles affect our quality of life through many different environmental related processes like public health [e.g., *Donaldson et al.*, 1998], and climate change patterns [e.g., *Charlson et al.*, 1987]. The formation and growth of atmospheric aerosols are key processes describing and determining their dynamics [see, e.g., *Kulmala et al.*, 2000]. In order to be able to better understand the health and climatic effects of atmospheric aerosols, their formation processes should also be better understood. Formation of ultrafine particles detected at a few (3–5) nm, and subsequent growth even to ~100 nm in 1–2 days, has been observed frequently in the continental boundary layer. Such observations span from northernmost subarctic Lapland, over the remote boreal forest [*Mäkelä et al.*, 1997; *Kulmala et al.*, 1998] and suburban Helsinki [*Väkevä et al.*, 2000], to industrialized agricultural regions in Germany [*Birmili and Wiedensohler*, 1998, 2000]. In coastal environments around Europe [*O'Dowd et al.*, 1999] very extensive formation bursts have been observed.

[3] For quantification and predictive purposes, it is important to understand the key processes leading to the formation and evolution of atmospheric aerosols. In this study a recently developed analytical method [*Kulmala et al.*, 2001b] has been developed further, and then used to obtain physical and chemical insight into natural aerosol formation processes. With the simple analytical method we have estimated (1) the concentration and source strength of condensable vapor leading to observed particle growth, and (2) the formation rate of 3 and 1 nm particles as well as the number concentration of 1 nm particles. This analysis is performed using only ambient aerosol size distribution data during nucleation and growth events with particular attention to the concepts of condensation and coagulation sinks.

[4] Our method is used to evaluate new particle and growth events observed (1) at coastal environment, where the PARFORCE (New Particle Formation and Fate in the Coastal Environment) project was conducted from 1998 to

[1] Also at Institute of Physics, Tampere University of Technology, Tampere, Finland.
[2] Also at Department of Physics, National University of Ireland, Galway, Ireland.

0148-0227/02/2001JD001053$09.00

2000 [*O'Dowd et al.*, 2002a, 2002b] and (2) in the boreal forest regions where the BIOFOR (Biogenic Aerosol Formation Over the Boreal Forest) project was conducted from 1998 to 2000 [*Kulmala et al.*, 2001a]. Two PARFORCE intensive field campaigns took place in Mace Head in the coastal site in West Ireland. Three BIOFOR intensive field campaigns took place in Hyytiälä in the boreal forest region of central southern Finland. Hyytiälä is also the site for the Finnish SMEAR II station (Station for Measuring forest Ecosystem-Atmospheric Relations) hosting continuous long–term monitoring of atmospheric processes such as turbulent fluxes and aerosol physicochemical interactions, which allow the general BIOFOR results to be viewed in the context of annual cycles and interannual variability.

2. Theory

[5] The aim of the model development is to derive a simple analytical method to estimate the concentration of condensable vapor and its source rate, by using the observed nucleation mode growth rate and measured size distributions. Furthermore, the analysis also provides an estimate to the nucleation rate.

[6] The particle size distribution n is described in detail by the general dynamic equation (GDE) [see *Seinfeld and Pandis*, 1998]

$$\begin{aligned}\frac{\partial n(d_p,t)}{\partial t} = {} & \frac{1}{2}\int_{d_{p0}}^{\left(d_p^3-d_{p0}^3\right)^{1/3}} \left(\beta\left(\left[d_p^3-d_p'^3\right]^{1/3},d_p'\right)\right. \\ & \left.\times\, n\left(\left[d_p^3-d_p'^3\right]^{1/3},t\right)n\left(d_p',t\right)dd_p'\right) \\ & -n(d_p,t)\int_{d_{p0}}^{\infty}\beta\left(\left[d_p,d_p'\right]\right)n(d_p,t)n\left(d_p',t\right)dd_p' \\ & -\frac{\partial}{\partial d_p}\left[\frac{dd_p}{dt}n(d_p,t)\right] \\ & +J(d_p)\delta(d_p-d_{p0}), \end{aligned} \tag{1}$$

in which the third and fourth terms on the right-hand side describe condensation and nucleation, respectively. The first term on the right–hand side is the coagulation production term, i.e., the formation rate of particles of radius d_p from smaller particles. The second term is the coagulation loss term, i.e., the removal rate of particles of radius d_p because of collisions with particles of any size. J is the nucleation rate and β the collision frequency function. The growth rate of the particle diameter in the condensation term can be calculated from

$$\frac{dd_p}{dt} = \frac{4m_v\beta_m DC_{vapor}}{d_p\rho}. \tag{2}$$

Here m_v is the molecular mass of the condensable vapor, β_m is the transitional correction factor for the mass flux, D is the diffusion coefficient and ρ is the particle density.

[7] Coupled with the GDE, one has to solve a balance equation also for the condensable vapor:

$$\frac{dC_{vapor}}{dt} = Q - CS \times C_{vapor} \tag{3}$$

where Q is the source rate and CS is the condensation sink. The condensation sink is the value of how rapidly condensable vapor molecules will condense on the existing aerosol (the whole particle size distribution). Its unit is 1/s. It is obtained from

$$CS = 2\pi D\int_0^{\infty} d_p\beta_m(d_p)n(d_p)dd_p = 2\pi D\sum_i \beta_i d_{pi}N_i \tag{4}$$

[see also *Pirjola et al.*, 1999], where d_{pi} is the diameter of a particle in size class i and N_i is the particle concentration in the respective size class. We adopt the transition regime correction factor β_m from *Fuchs and Sutugin* [1971].

$$\beta_m = \frac{1+Kn}{1+\left(\frac{4}{3\alpha_m}+0.337\right)Kn+\frac{4}{3\alpha}Kn^2,} \tag{5}$$

where α is the sticking coefficient, and a dimensionless group, the Knudsen number, is

$$Kn = \frac{2\lambda}{d_p}. \tag{6}$$

Here λ is the effective mean free path of the vapor molecules in the gas and thus the Knudsen number is the ratio of two length scales, a length scale λ characterizing the gas with respect to the transport of mass and a length scale d_p characterizing the droplet. From simple kinetic theory of gases, the 0th order approximation for λ can be expressed by means of a measurable macroscopic property like diffusion coefficient (D) and the average absolute velocity of the vapor molecules [e.g., *Hirshfelder et al.*, 1954].In the equation, it has been assumed that the condensable vapor does not take part in nucleation, i.e., it is a different vapor or combination of vapor that nucleates, and the condensable vapor under study is depleted only because of its condensation onto existing particles.

[8] Well–established numerical methods to solve the GDE exist [e.g., *Gelbard and Seinfeld*, 1980; *Raes and Janssens*, 1986; *Jokiniemi et al.*, 1994; *Jacobsson and Turco*, 1995]. However, in this case we are looking for simple, analytical order-of-magnitude estimates, which also provide insight into the relative importance of different aerosol dynamical mechanisms. Thus, we will first simplify equation (1) by neglecting terms, based on simple order of magnitude analysis. Since the collision frequency function β is much larger for particles of uneven size than for similar size, we can neglect the coagulation production term (compared with the coagulation loss term). Furthermore, it can be shown from the experimental results shown later that the coagulation production term, which in this context can also be called the self-coagulation term, is much smaller than the production term by condensation (which in the experiments is always of the order nm/h or above). This can be seen by

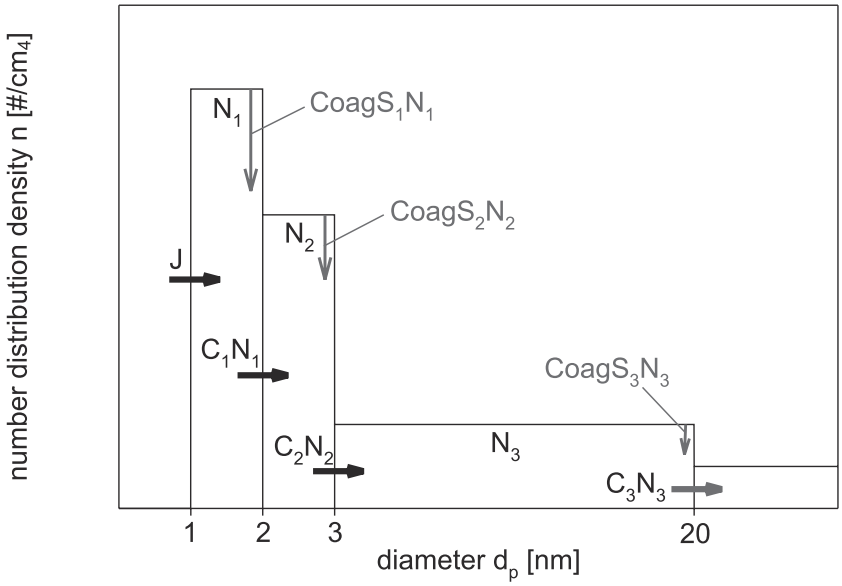

Figure 1. The division of the particle size spectrum into classes. Number distribution density n_i in each class is assumed constant. N_i is the total number concentration in class i. The particle fluxes to and from each class is indicated by arrows: J is the nucleation rate, C_iN_i the condensational particle flux from class i to the next class, and $CoagS_iN_i$ the rate by which the concentration of class i decreases by coagulation with other particles.

using the monodisperse coagulation model as quantifying the self-coagulation rate, resulting in the approximation

$$\frac{dd_p}{dt} = \frac{d_p \beta N}{6} \tag{7}$$

Hence, by inserting representative (upper estimate) values for the variables (diameter d_p = 3 nm, collision frequency function $\beta = 10^{-9}\mathrm{cm}^3/\mathrm{s}$, total nucleation mode number concentration $N = 10^5$ 1/cm^3), the resulting growth rate is 0.18 nm/h, which is clearly lower than the condensational growth rate.

[9] This neglection simplifies the GDE greatly since it reduces to the form

$$\begin{aligned}\frac{\partial n(d_p,t)}{\partial t} = &-n(d_p,t)\,CoagS(d_p,t)\\ &-\frac{\partial}{\partial d_p}\left[\frac{dd_p}{dt}n(d_p,t)\right]\\ &+J(dp)\delta(d_p-d_{p0}).\end{aligned} \tag{8}$$

[10] Thus the coagulation term was simplified to the product of $n(d_p)$ and a coagulation sink

$$CoagS(d_p,t) = \int_{d_{p0}}^{\infty} \beta\left(d_p,d'_p\right) n\left(d'_p,t\right) dd'_p. \tag{9}$$

Next, equation (8) is transformed into discrete form. To do this, four size classes (based on particle diameter) are introduced: (1) 1–2 nm, (2) 2–3 nm, (3) 3–20 nm, and (4) >20 nm. The number concentration density functions in the classes n_1, n_2, n_3 and n_4 are assumed constant, i.e., within the size class they do not depend on size. Then, if we set $N_i = n_i \Delta d_{pi}$ to be the total number concentration of each size class, we get by integrating equation (8) over size classes 1, 2 and 3 the following concentration balance equations:

$$\frac{dN_1}{dt} = J - CoagS_1N_1 - C_1N_1 \tag{10}$$

$$\frac{dN_2}{dt} = C_1N_1 - CoagS_2N_2 - C_2N_2 \tag{11}$$

$$\frac{dN_3}{dt} = C_2N_2 - CoagS_3N_3 - C_3N_3, \tag{12}$$

in which

$$C_i = \frac{1}{\Delta d_{pi}}\frac{dd_p}{dt}\Big|_{d_p=d_{pi}} = \frac{4m_v\beta_i DC_{vapor}}{\rho d_{pi}\delta d_{pi}}. \tag{13}$$

[11] These production and loss terms of these equations are also graphically illustrated in Figure 1. The production term for size class 1 is nucleation, i.e., the size of nucleating particles is assumed to be 1 nm. There are two loss terms, one because of coagulation with preexisting particles, the other because of growth into class 2. The coagulation sink of size class i is calculated from the experimental data, using equation (9) for diameter d_{pi}. The production and loss terms of classes 2 and 3 follow this same logic.

[12] The concentration of condensable vapor C_{vapor} can be obtained by integrating equation (2) from d_{p0} to d_p (assuming constant C_{vapor} during growth) [*Kulmala*, 1988]:

$$\begin{aligned}C_{vapor} = \frac{\rho}{\Delta t D m_v}\times\Bigg[&\frac{d_p^2-d_{p0}^2}{8}+\left(\frac{4}{3\alpha}-0.623\right)\frac{\lambda}{2}(d_p-d_{p0})\\ &+0.623\lambda^2\ln\frac{2\lambda+d_p}{2\lambda+d_{p0}}\Bigg].\end{aligned} \tag{14}$$

[13] Here the mass accommodation coefficient (i.e., sticking coefficient) is α and λ is the mean free path. This gives

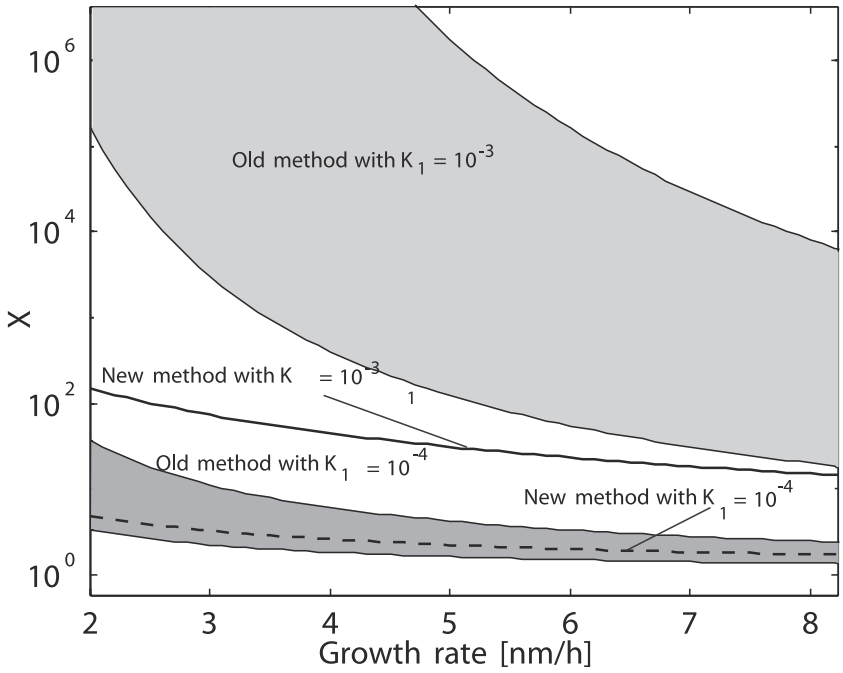

Figure 2. The sensitivity of the data analysis methods to variations in the growth rate and coagulations sinks. The upper, vertically shaded area corresponds to the estimates given by the older method if $K_1 = 10^{-3}s^{-1}$, and the dotted area to the old method with $K_1 = 10^{-4}s^{-1}$. The solid and dashed lines shows the new method results, the solid one corresponding to the higher sink value.

us then also the source rate of condensable vapor, directly from equation (3).

[14] One approximation that we make in the analysis is that the coagulation sink in each of the classes is calculated using one representative size of the class. In this case, we chose the lower end of each class for this, i.e., the sink for class 1 is calculated using 1nm as the particle diameter, and so on. Also, in the following analysis, we employ two further assumptions. The concentration of condensable vapor, as well as the smallest sizes are assumed to be in pseudo steady state, i.e., C, N_1 and N_2 are assumed constant during the nucleation burst. Furthermore, the particle flux out of the nucleation mode because of condensation C_3N_3 is assumed negligible. With these assumptions, the above equations reduce to

$$N_1 = \frac{J}{C_1 + CoagS_1} \tag{15}$$

$$N_2 = \frac{JC_1}{(C_1 + CoagS_1)(C_2 + CoagS_2)} \tag{16}$$

$$\frac{dN_3}{dt} = \frac{\Delta N_3}{\Delta t} = C_2N_2 - CoagS_3N_3. \tag{17}$$

[15] In these equations, we have only three unknowns: N_1, N_2 and J. The rest can be found from the experiments. The solution for the nucleation rate J gives

$$J = \frac{(CoagS_1 + C_1)(CoagS_2 + C_2)}{C_1C_2}\left[\frac{\Delta N_3}{\Delta t} + CoagS_3N_3\right]. \tag{18}$$

[16] This analysis provides a more rigorous treatment of the condensation and coagulation processes of small particles than the method presented by *Kulmala et al.* [2001b]. In the earlier version of the method J was estimated from

$$J = e^{KT}\left[\frac{\Delta N_3}{\Delta t} + N_3K_3\right], \tag{19}$$

where K is a mean coagulation sink for particles growing from 1 nm to the 3 nm detection limit, and T is the time needed for this growth. In practice K was taken to be the arithmetic mean of K_1 and K_2. The part in the square brackets is the same in both methods, and the multiplying factor has changed. In the following we concentrate on this factor. Figure 2 shows the behavior of the multiplier of both methods for growth rates and coagulation sinks typical in the boreal forest. For this figure we assumed $K_2 = \frac{K_1}{3}$, and plotted the sensitivity of the two methods to the growth rate. The shaded areas show the value of e^{KT} when K ranges form K_1 to K_2. The upper area corresponds to $K_1 = 10^{-3}$ s^{-1} and the lower to $K_1 = 10^{-4}$ s^{-1}. One can see that the uncertainty in the previous method is unreasonably large especially for the higher coagulation sink. The lines in the figure show the behavior of the multiplier of the new method, again with $K_1 = 10^{-3}$ s^{-1} (solid line) $K_1 = 10^{-4}$ s^{-1} (dashed line). We see that changing the coagulation sink by a factor of 10 results in a change in J which is the same magnitude. The new method is less sensitive to uncertainties in the growth rate, and in addition removes the error that the use of a "mean coagulation sink" caused.

3. Measurements and Data Analysis

3.1. Instrumentation

[17] During the BIOFOR and PARFORCE campaigns, the total particle concentration was measured using two

Condensation Particle Counters (CPC) in parallel. The TSI model 3025 measured concentrations at sizes over 3 nm, and the model 3010 over 10 nm. Small particle number size distributions were measured using a dual DMPS (Differential Mobility Particle Sizer) system, which during BIOFOR covered size range 3–10 nm and 10–500 nm and during PARFORCE campaign size range 3–15 nm and 15–800 nm. The calibration procedures and sampling system during BIOFOR campaign is described by *Aalto et al.* [2001] and during PARFORCE campaign by *O'Dowd et al.* [2002a]. During the BIOFOR period the particles measured with DMPS were considered as dry, dehydrated particles, and the measured sizes were later converted to "ambient," hydrated sizes using particle growth factors, experimentally measured with a Tandem Differential Mobility analyzer (TDMA) [*Hämeri et al.*, 2001]. However, aerosol humidity during the DMPS measurements might have been as high as 50% which means that particles are not totally dehydrated. During PARFORCE period aerosol humidity inside the DMPS was always less than 30% and particles were also assumed to be totally dehydrated. This time we did not have any experimentally measured growth factors available.

[18] The large particle number size distributions were measured using in situ optical particle counters. During BIOFOR sizes from 100 nm to 3 μm were measured using a Particle Measuring System's (PMS) Active Scattering Aerosol Spectrometer Probe (ASASP). Sizes from 0.5 μm to 32 μm were measured with a PMS Classical Scattering Aerosol Spectrometer Probe (CSASP-100). During PARFORCE, a PMS Forward Scattering Spectrometer Probe (FSSP) and an Optical Array Probe (OAP) were used to determine ambient aerosol spectra from 0.5 micrometers up to 300 micrometers. During both campaigns probes were mounted on a tower on a rotating mount which ensured that sampling was always conducted parallel to the local wind direction. The PMS probes measure aerosols in an nonintrusive manner and under ambient relative humidity conditions.

3.2. Data Analysis

3.2.1. Condensation and coagulation sinks

[19] The measured particle number size distributions were used to calculate the condensation and coagulation sinks for the measurement campaign periods. As the DMPS measure the dry sizes of the particles, we multiplied the sizes of the DMPS data with a growth factor in order to get more realistic sink values. For the forest environment (BIOFOR), we used experimentally measured growth factors for different size classes, given by *Hämeri et al.* [2001], to get an "ambient" particle size distribution. The optical particle counters measured the particles at their wet sizes, so for them there was no need for this procedure. For the coastal data (PARFORCE) we did not have growth rate data for the particles measured with the DMPS (Aitken mode or accumulation mode), so we used two different growth factors, namely 1.0 and 1.5, to estimate the ambient size distribution. These values roughly correspond to the experimentally found lower and upper limits by *Hämeri et al.* [2001]. The condensation sink was then obtained by calculating the Knudsen number and the transitional correction factor for each size class, and then integrating it according to *Pirjola et al.* [1999]. The calculated data was then combined in time series covering the whole campaign periods.

[20] The time resolution used was that of the optical particle counter's, when the data was available. The DMPS data for each time value was taken from the closest measurement.

[21] Unfortunately, optical particle counter data was available only for some days of the BIOFOR period, so for the time series we used only DMPS data. From the data available we conclude that this underestimates the total sink by ~5% of the actual value in the forest environment.

[22] We also calculated the condensation sink using several different values for the sticking coefficient α, to get a picture of its effect on the total value and size distribution.

[23] The coagulation sink was calculated in much the same way, using the same "grown" DMPS data as for the condensation sink. We calculated the coagulation coefficient for particles of 1, 2, and 3 nm diameters with every measured size class, and summed over the whole measured spectrum (for more details, see *Kulmala et al.* [2001b]).

3.2.2. Formation and growth rate of new particles

[24] We chose four days for a closer analysis using this analytical technique of the formation and growth rate of newly formed particles. Two of these are from during the BIOFOR 3 campaign in Hyytiälä and two from PARFORCE, Mace Head. For all of these the size distribution data show a clear increase in the number concentration of <10 nm particles. Those particles also growth to Aitken mode size during the afternoon and towards the evening every day except for one of the coastal cases (JD 165). This day was a so-called Type I event (clean event), where it is assumed that the source of particle production is a very local, tidal region ~100 m away from the measuring station. Type III events (like JD 175.99) are polluted events, where the source region is at least 1–3 km from the station [*O'Dowd et al.*, 2002a, 2002b]. The observed formation rate of 3 nm particles was calculated as an average over the nucleation period, in order to decrease the effect of the fluctuations in the lowest channels of the DMPS.

[25] We took the number concentration of particles at the end of the particle formation period, when the particles already have grown into the more reliable size range of the instrument. From this we subtracted the particle number concentration just before the formation period, getting the number of new particles, N_{3-20}. To minimize the effect of background aerosol variation, we took into account only particles smaller than the maximum diameter that the newly nucleated particles had reached by the end of the formation period.

[26] For forest environment data, we used a MATLAB program to visually determine the start and end times of the new particle formation period, and also the largest size the particles had reached during the period. Using this information we obtained the formation rate and concentration of newly formed particles.

[27] The growth rate of new particles was estimated visually from the DMPS data plots. Due to the somewhat inaccurate nature of this method, we used a range of values for the calculations where it was needed. For the coastal

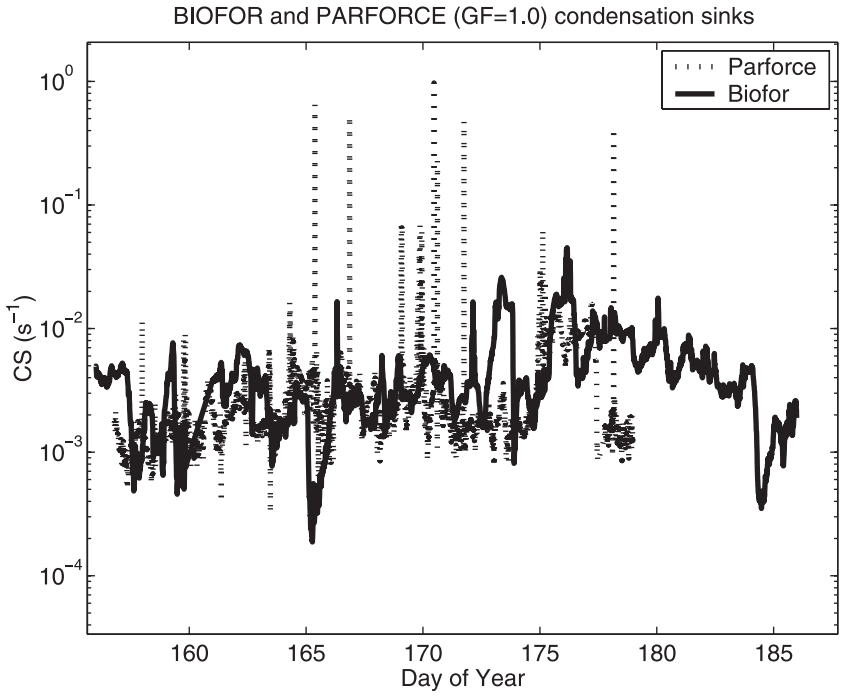

Figure 3. The total condensation sink as a function of time for both the BIOFOR and PARFORCE field campaign periods in 1999. The BIOFOR data has been shifted forward in time to fit it in the same figure.

case day JD 165, we used an estimate based on the assumption that the new particles were of 1 nm diameter and grew to a detectable size in the time needed to travel from the source to the measurement site (which was ~25 seconds in this case).

[28] We used equation (18) combined with equation (14) to calculate J for a range of growth rates and for the coastal case also several different growth factors. The coagulation sinks needed for the calculations were taken as averages over the nucleation periods.

4. Results and Discussion

4.1. Condensation Sinks

[29] Figure 3 shows the time series for both the forest environment (BIOFOR) and coastal (PARFORCE) field campaigns. The forest data has been time shifted to start at the same time as the coastal data. During both campaigns, the sinks varied between 10^{-4} and 4×10^{-2} s^{-1}, except for some peaks during the PARFORCE campaign, when the sink rises up to 10^{-1} s^{-1}. Most of these peaks can be associated with strong nucleation bursts, when the total particle concentrations rise to very high values and contributed significantly to the condensation sink.

[30] In Table 1 the mean, median and upper and lower quartiles and the 10th and 90th percentiles for both measurement sites are presented. The values for coastal data are given for two growth factors of 1.0 and 1.5 since we did not have data for the actual growth factors. While the mean value of the forest data falls between the means for the coastal data, the median value is higher than both of them. This might be due to the very high peak values of the coastal condensation sink, which occurs during the intensive particle formation periods, and increase the mean value.

[31] The mean diurnal behavior of the condensation sink is plotted in Figure 4. The forest data show generally higher sinks than the coastal data by a factor of 2–3. In the forest environment data, one can see that the sink value drops to its daily minimum around noontime, the time when most particle formation events start.

[32] The coastal sink daily mean also shows a drop around midday, but the condensation sink then rises again. This is caused by the new particles, growing to bigger sizes and adding to the sink.

[33] The condensation sink as a function of size for both a coastal and a forest event day are presented in Figure 5, and a clear difference can be seen. The contribution of >800 nm particles to the total sink is significant in the coastal data, whereas in the forest environment the concentrations of those particles is too small to affect the total sink value. If we look at the situation with a sticking coefficient of 0.01, this effect is even more pronounced. A smaller sticking coefficient lowers the total sink value, but increases the relative contribution of larger particles to the sink. The coagulation sinks for 1, 2, and 3 nm particles typically follow dynamical behavior of condensation sinks as seen in

Table 1. Statistics for the Condensation Sinks (10^{-3} s^{-1}) in PARFORCE and BIOFOR

Data Set	GF	Mean	Median	P_{10}	P_{25}	P_{75}	P_{90}
PARFORCE 99	1.0	3.32	1.87	1.18	1.45	3.28	7.56
PARFORCE 99	1.5	5.48	3.05	1.88	2.36	5.05	14.0
BIOFOR 3	Measured	4.77	3.61	1.12	2.17	5.37	9.38

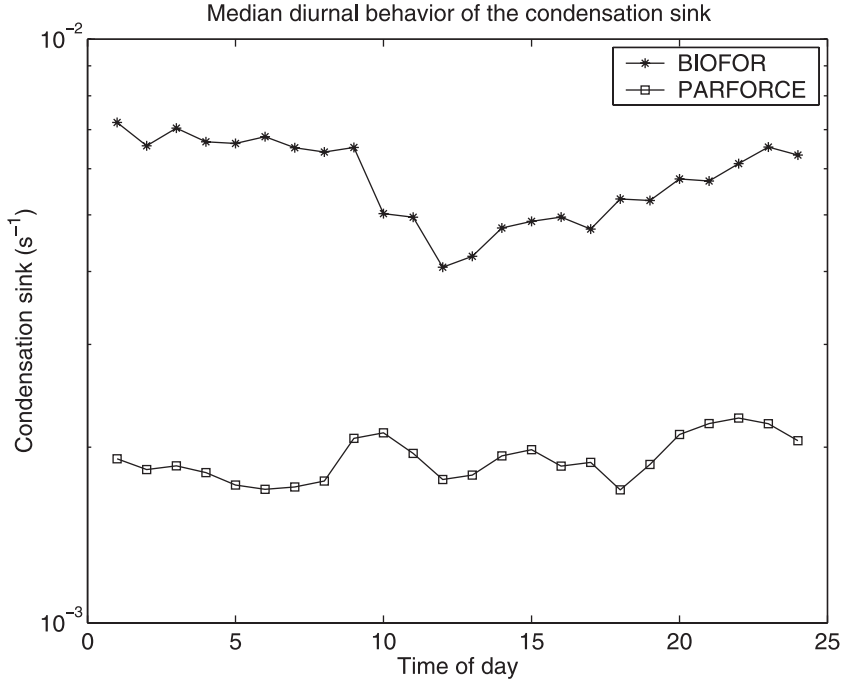

Figure 4. Diurnal behavior of the condensation sink during BIOFOR and PARFORCE campaigns. The sink value of was averaged over each hour of the day, and of these values the shown values were computed. The BIOFOR sink values show a drop around noon, reaching its minimum at the time most events start. PARFORCE data does not show this behavior.

Figure 6. The peaks around noon occurred at the same time for all tree coagulation sinks as well as for condensation sink.

4.2. Comparison of Forest and Coastal Cases

[34] The formation rate and concentration of 1 nm particles have been estimated using equations (15)–(18) and vapor concentrations and its source rate have been estimated using equations (2)–(3). In Table 2 the comparison of 2 boreal forest days and 2 coastal days are given. The results for the forest event days are very similar, J falling into the range of 8–20 s^{-1} cm^{-3}. The production rate in coastal environment was much higher for both case days studied.

[35] During the forest event on JD 96 in BIOFOR the observed 3 nm particle formation rate was 1.6×10^{-1} s^{-1} cm^{-3}. The coagulation sink was close to 5×10^{-4} for 3 nm particles during the event. It is notable that the sink data show a significant drop in the total condensation and coagulation sinks during the event period. Using these sinks and the corrected ambient (wet) size distribution we got J_1 to be from 6–15 s^{-1} cm^{-3}, in the growth rate range from 2 nm/h to 4 nm/h. The concentration of 1 nm particles, N_1, was estimated to be 2000–6000 cm^{-3}.

[36] The estimated condensable vapor concentration was $2–5 \times 10^7$ cm^{-3}. Using equation (1), assuming steady state situation we were able to obtain the vapor source rate to be about 10^5 cm^{-3} s^{-1}.

[37] In the forest event on JD 104 the observed 3–20 nm particle formation rate was 0.18 s^{-1} cm^{-3}. The coagulation sink data were very similar to JD 96, and consequently the value for J_1 obtained was between 5 and 20 particles per cc per second, and the concentration of new particles during the event was about the same as for the other forest event day, as well as the vapor source rate.

[38] During the coastal events on JD 165 and JD 175 in PARFORCE the aerosol bursts were much stronger than during the forest events. During the type I event on JD 165 taking the observed formation rate of new particles to be ~20,000 s^{-1} cm^{-3}, and the growth rate between 120 and 180 nm/h, we got J_1 to be 2.2×10^4 s^{-1} cm^{-3}. Figure 7 shows the sensitivity of J_1 to the growth rate once again, this time using the conditions of JD 165 and JD 175 in PARFORCE. The estimate for J_1 is quite insensitive to changes in the growth rate in this case. In practice, when the condensational growth rate is more than 100 nm/h then J_1 is about the same as the formation rate of new particles. This holds also for the peak formation rates, which were as high as 200,000 s^{-1} cm^{-3}. The coagulation sinks were slightly higher than in the forest cases, but in this case the coagulation processes did not have enough time to remove but about 10% of the particles before they reached detectable sizes.

[39] The number concentration of 1 nm particles was estimated to be $2 \times 10^5–7 \times 10^6$ cm^{-3}, and the vapor source rate estimated from the growth rate is around $4–5 \times 10^6$ cm^{-3} s^{-1}.

[40] During the PARFORCE Type III coastal (polluted) event on JD 175, we estimated the growth rate to be 15–20 nm/h. The coagulation sinks were ~3–5 times higher than in the previous cases, depending on the assumed hydroscopic growth factor. A J_1 estimate of 400––1000 s^{-1} cm^{-3} was computed. Even though the growth rate was significantly higher than in the boreal forest cases, coagulation had time to

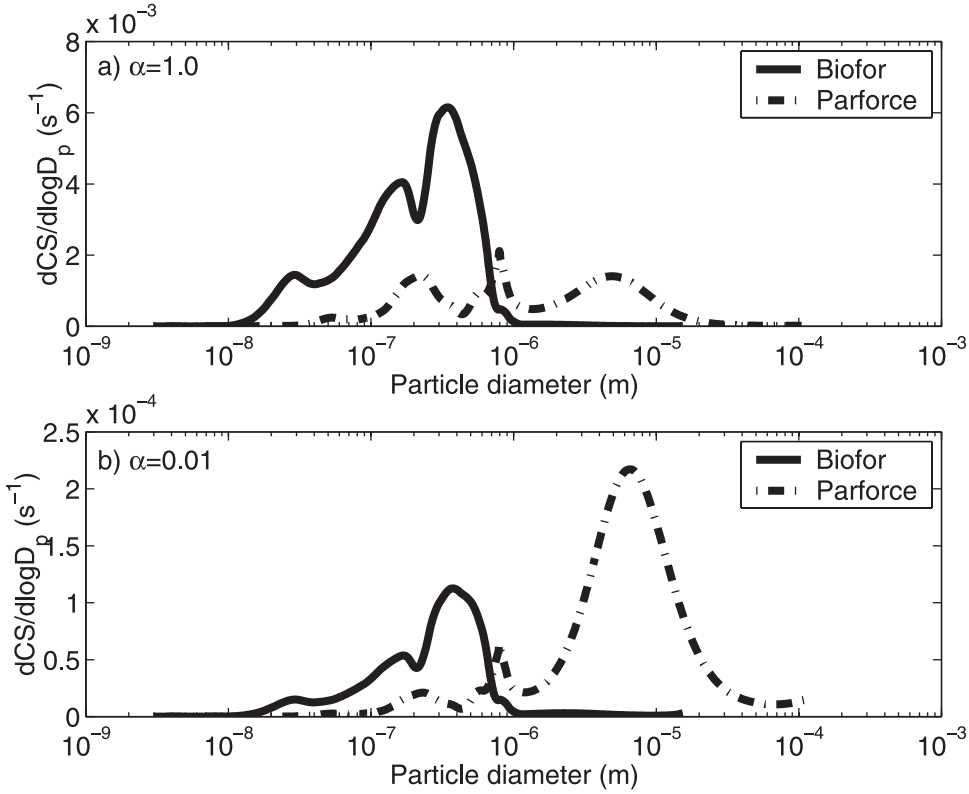

Figure 5. The condensation sink as a function of size. For the BIOFOR data we used measured growth factors for the DMPS data, and the PARFORCE growth factor of submicrometer particles is assumed to be 1.0. The upper picture shows the sink computed with a sticking coefficient of unity, in the lower one it is 0.01.

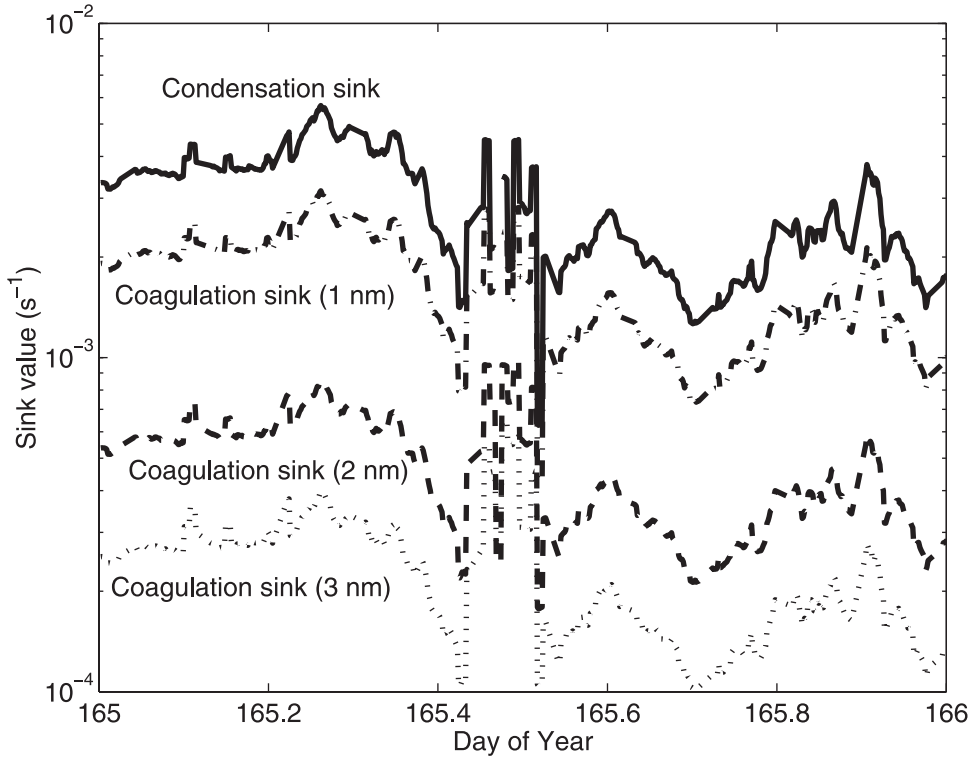

Figure 6. The values of the condensation and coagulation sinks during a PARFORCE event day. The value of the condensation sink is the highest, and the coagulation sink decreases when the respective particle size increases. Since all sinks depend strongly on the size distribution of the preexisting particles, the time behavior is very similar, the only difference being the order of magnitude of the sink value.

Table 2. Summary of the Results Calculated in This Study

Day	N_3 $[cm^{-3}]$	$\frac{dN^3}{dt}$ $[cm^{-3}s^{-1}]$	J_1 $[cm^{-3}s^{-1}]$	N_1 $[cm^{-3}]$	$\frac{dr}{dt}$ $[nm/h]$	Q $[10^5 cm^{-3}s^{-1}]$	C $[10^7 cm^{-3}]$
JD 94, BIOFOR	2.5×10^3	1.6×10^{-1}	8–20	2×10^3–6×10^3	2–4	1.1–2.2	2.6–5.2
JD 104, BIOFOR	3.4×10^3	1.8×10^{-1}	8–20	2×10^3–5×10^3	2–4	1.0–2.0	2.6–5.2
JD 165, PARFORCE	3.0×10^5	10^4–10^5	10^4–10^5	2×10^5–7×10^6	120–180	34–52	150–230
JD 175, PARFORCE	1.5×10^4	100	400–10^3	4×10^4–10^5	15–20	10–24	20–26

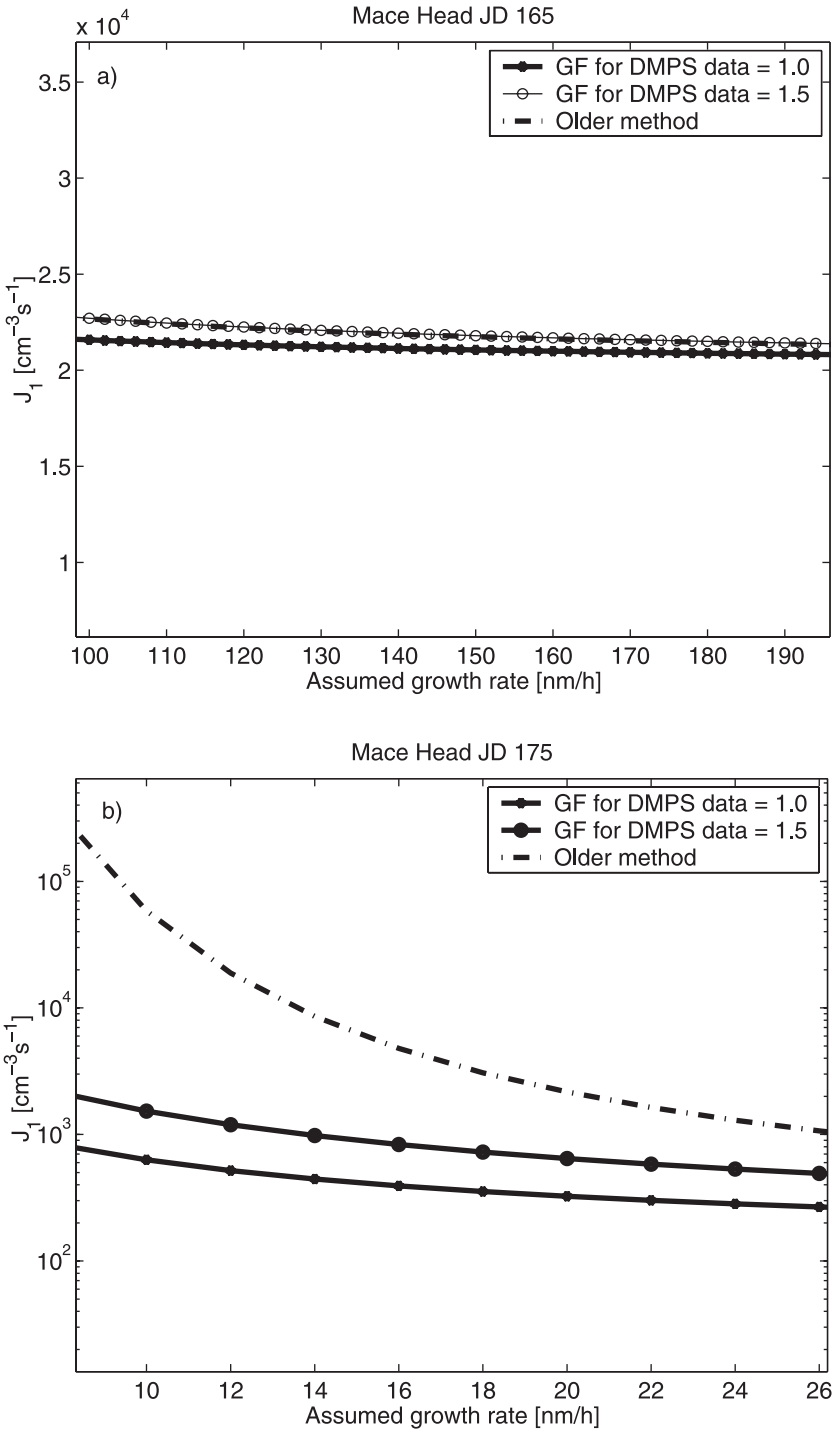

Figure 7. The sensitivity of the 1 nm particle nucleation rate to estimates of growth rate and hydroscopic growth factor in PARFORCE on JD 165 (a) and 175 (b).

remove a significant part of the newly formed particles before they reached the detection limit. In this case, due to the relatively high coagulation sink, the difference compared to the formerly used analysis method is quite large, as can be seen in Figure 7b. One can see that the new method gives an order of magnitude smaller J_1 for the growth rate range that we assumed. The computed condensable vapor source rate is $1-2 \times 10^6$ cm^{-3} s^{-1}. Number concentration of 1 nm particles was estimated to be $0.4-4 \times 10^5$ cm^{-3}.

[41] The estimation boundaries include the effect of the hydroscopic growth factor on the coagulation sinks. In the coastal case on JD 165 the growth factor has little effect as coagulation is hardly significant. On JD 175 the increase of the growth factor from 1.0 to 1.5 increases J_1 by almost a factor of 2.

5. Conclusions

[42] Using only the measured evolving size spectra of atmospheric aerosols together with condensation and coagulation sinks and condensation growth rates, we are able to obtain an order of magnitude estimate for the: (1) concentration of condensable vapor; (2) source rate of vapor molecules; (3) formation rate of 3 nm particles; (4) formation rate of 1 nm particles, and (5) number concentration of 1 nm particles.

[43] In this study we have developed a new, more robust version, of the recently developed analytical theoretical tool [*Kulmala et al.*, 2001b] to estimate nucleation rates (or formation rate of 1 nm particles) in the atmosphere.

[44] Using this tool, we have presented aerosol condensation and coagulation sink data for the coastal boundary layer aerosol and compared this to boundary layer aerosol sinks observed over the boreal forest. The coagulation and condensation sinks are typically somewhat higher in the forest environment; however, there are several very high sink values encountered during strong coastal nucleation events. In all cases the diurnal variation of condensation and coagulation sinks is similar. In the coastal environment, coarse mode particles have a significant effect on the aerosol condensation sink value, in contrast to forest environment where only the Aitken and accumulation modes have an important effect. The estimated 1 nm nucleation rates, as well as number concentrations of 1 nm particles are significantly higher in the coastal environment when compared to the forest environment. The high particle growth rates in the coastal air imply also greater condensable vapor concentrations than in the forest, and also suggest that the vapor source rates are greater at the coast.

References

Aalto, P., et al., Physical characterization of aerosol particles during nucleation events, *Tellus, Ser. B*, *53*, 344–358, 2001.

Birmili, W., and A. Wiedensohler, The influence of meteorological parameters on ultrafine particle production at a continental site, *J. Aerosol Sci.*, *29*, 1015–1016, 1998.

Birmili, W., and A. Wiedensohler, New particle formation in the continental boundary layer: Meteorological and gas phase parameter influence, *Geophys. Res, Lett.*, *27*, 3325–3328, 2000.

Charlson, R., J. Lovelock, M. Andreae, and S. Warren, Oceanic phytoplankton, atmospheric sulphur, cloud albedo and climate, *Nature*, *326*, 655–661, 1987.

Donaldson, K., X. Li, and W. MacNee, Ultra-fine (nanometer) particle-mediated lung injury, *J. Aerosol. Sci.*, *29*, 553–560, 1998.

Fuchs, N., and A. Sutugin, Highly dispersed aerosol, in *Topics in Current Aerosol Research*, edited by G. Hidy and J. Brock, Pergamon, New York, 1971.

Gelbard, F., and J. Seinfeld, Coagulation and growth in multicomponent aerosol, *J. Colloid Interface Sci.*, *78*, 485–501, 1980.

Hämeri, K., M. Väkevä, P. Aalto, M. Kulmala, E. Swietlicki, W. Seidl, E. Becker, and C. O'Dowd, Hygroscopic and CCN properties of aerosol particles in boreal forests, *Tellus, Ser. B*, *53*, 359–379, 2001.

Hirshfelder, J., C. Curtiss, and R. Bird, *Molecular Theory of Gases and Liquids*, John Wiley, New York, 1954.

Jacobsson, M., and R. Turco, Simulating condensational growth, evaporation, and coagulation of aerosols using a combined moving and stationary size grid, *J. Aerosol. Sci.*, *22*, 73–92, 1995.

Jokiniemi, J., M. Lazaridis, K. Lehtinen, and E. Kauppinen, Numerical simulation of vapour-aerosol dynamics in combustion processes, *J. Aerosol Sci.*, *25*, 429–446, 1994.

Kulmala, M., Nucleation as an aerosol physical problem, Ph.D. thesis, Dep. of Phys., Univ. of Helsinki, Helsinki, Finland, 1988.

Kulmala, M., A. Toivonen, J. Mäkelä, and A. Laaksonen, Analysis of the growth of nucleation mode particles observed in boreal forest, *Tellus, Ser. B*, *50*, 449–462, 1998.

Kulmala, M., L. Pirjola, and J. Mäkelä, Stable sulphate clusters as a source of new atmospheric particles, *Nature*, *404*, 66–69, 2000.

Kulmala, M., et al., Overview of the international project on biogenic aerosol formation in the boreal forest (BIOFOR), *Tellus, Ser. B*, *53*, 324–343, 2001a.

Kulmala, M., M. Dal Maso, J. M. Mäkelä, L. Pirjola, M. Väkevä, P. Aalto, P. Miikkulainen, K. Hämeri, and C. O'Dowd, On the formation, growth and composition of nucleation mode particles, *Tellus, Ser. B*, *53*, 479–490, 2001b.

Mäkelä, J., et al., Observations of ultrafine aerosol particle formation and growth in boreal forest, *Geophys. Res. Lett.*, 1219–1222, 1997.

O'Dowd, C., et al., On the photochemical production of new particles in the coastal boundary layer, *Geophys. Res. Lett.*, *26*, 1707–1710, 1999.

O'Dowd, C., et al., A dedicated study of new particle formation and fate in the coastal environment (PARFORCE): Overview of objectives and initial achievements, *J. Geophys. Res.*, *107*, 10.1029/2001000555, in press, 2002a.

O'Dowd, C., et al., Coastal new particle formation: Environmental conditions and aerosol physicochemical characteristics during nucleation bursts, *J. Geophys. Res.*, *107*, 10.1029/2000000206, in press, 2002b.

Pirjola, L., M. Kulmala, M. Wilck, A. Bischoff, F. Stratmann, and E. Otto, Effects of aerosol dynamics on the formation of sulphuric acid aerosols and cloud condensation nuclei, *J. Aerosol Sci.*, *30*, 1079–1094, 1999.

Raes, F., and A. Janssens, Ion-induced aerosol formation in a H2O-H2SO4 system, II, Numerical calculations and concusions, *J. Aerosol. Sci.*, *17*, 715–722, 1986.

Seinfeld, J., and S. Pandis, *Atmospheric Chemistry and Physics: From Air Pollution to Climate Change*, John Wiley, New York, 1998.

Väkevä, M., K. Hämeri, T. Puhakka, E. Nilsson, H. Hohti, and J. Mäkelä, Effects of meteorological processes on aerosol particle size distribution in an urban background area, *J. Geophys. Res.*, *105*, 9807–9821, 2000.

P. Aalto, M. Dal Maso, M. Kulmala, and K. E. J. Lehtinen, Department of Physical Sciences, P.O. Box 64, University of Helsinki, FIN-00014, Finland. (pasi.p.aalto@helsinki.f; miikka.dal@helsinki.fi; markku.kulmala@helsinki.fi; kari.lehtinen@helsinki.fi)

Jyrki M. Mäkelä, Institute of Physics, Tampere University of Technology, P.O. Box 692, Tampere FIN-33101, Finland. (jyrki.makela@tut.fi)

C. D. O'Dowd, Department of Physics, National University of Ireland, Galway, University Road, Galway, Ireland. (colin.odowd@cmas.demon.co.uk)